CrossMark

An Investigation into Quantum Chemistry and Experimental Evaluation of Imidazopyridine Derivatives as Corrosion Inhibitors for C-Steel in Acidic Media

Elhachmia Ech-chihbi[1,2] · Ayssar Nahlé[3] · Rajae Salim[1,2] · Hassan Oudda[1] · Fadoua El Hajjaji[2] · Fouad El Kalai[4] · Abdelmalik El Aatiaoui[4] · Mustapha Taleb[2]

Abstract
The corrosion inhibition performance of two imidazopyridine derivatives, namely 6-nitroso-2-phenylimidazo[1,2-a]pyridine-3 carbaldehyde (C1) and (2-phenylimidazo[1,2-a]pyridin-3-yl)methanol (C2) for carbon steel in 1.0 M hydrochloric acid solution, was evaluated using electrochemical impedance spectroscopy (EIS), potentiodynamic polarization, and quantum chemical calculations. The surface morphology was examined using Scanning Electron Microscopy (SEM). Imidazopyridine derivatives adsorbed onto the carbon steel surface via mixed types of adsorption with predominantly chemisorption obeying Langmuir adsorption isotherm. DFT computational chemistry at B3LYP/6-31G(d,p) basis set level was applied in order to correlate some electronic properties of tested molecules to the inhibition efficiencies obtained from experimental data. The computed Fukui functions have been useful to predict the reactive sites of nucleophilic and electrophilic attacks.

1 Introduction

Steel has found wide applications in a broad spectrum of industries to remove mill corrosion scales from metallic surfaces. The use of concentrated acid solutions (hydrochloric or sulfuric acid) at elevated temperature results in corrosion and eventually loss of metals [1–3]. A lot of attention has been given to the development of new and cost-effective organic compounds and studying their corrosion inhibition mechanism using several techniques [4]. The addition of organic corrosion inhibitors, which are compounds containing heteroatoms (=N–, –O-, and –S–), double and triple bonds, and aromatic rings, has been identified as one of the most practical and economical ways of corrosion control process of metals [5]. The mechanism of inhibition is generally explained by the formation of protective film on the surface of C-steel, which prevents diffusion of active corrosive anions from aggressive solution to the steel [6]. Many studies were done to evaluate the corrosion inhibition properties of different inhibitors in hydrochloric acid solutions using imidazopyridine derivatives [7–9].

In this work, the study focuses on new synthesized imidazopyridine derivatives, namely 6-nitroso-2-phenylimidazo[1,2-a]pyridine-3 carbaldehyde (C1) and (2-phenylimidazo[1,2-a]pyridin-3-yl)methanol (C2) as corrosion inhibitors for carbon steel in 1.0 M HCl solution. In a previous study, it was shown that imidazopyridine-type organic compounds are good corrosion inhibitors for many metals in aggressive media [10, 11] and they are also pharmacologically important and biologically active compounds which include several anxiolytic drugs [4, 12]. At the first stage of this study, the inhibitive behavior of the imidazopyridine derivatives was examined using chemical and electrochemical methods included weight loss, potentiodynamic polarization, and EIS techniques. In addition,

✉ Ayssar Nahlé
anahle@sharjah.ac.ae

1 Laboratory of Separation Processes, Faculty of Science, University Ibn Tofail, Kenitra, Morocco

2 Laboratory of Engineering, Electrochemistry, Modeling and Environment (LIEME), Faculty of Sciences, University Sidi Mohamed Ben Abdellah, Fez, Morocco

3 Department of Chemistry, College of Sciences, University of Sharjah, PO Box: 27272, Sharjah, United Arab Emirates

4 Laboratory of Applied Chemistry & Environment, Faculty of Science, Mohammed Premier University, B.P. 4808, 60046 Oujda, Morocco

the adsorption isotherm and quantum chemical studies were carried out to explore their adsorption type onto the metallic surface in search of new and efficient corrosion inhibitors [13]. On the other hand, the values of thermodynamic parameters were obtained from the adsorption isotherms and Arrhenius plots. The molecular structures of the studied inhibitors C1 and C2 are shown in Fig. 1.

2 Experimental Procedure

2.1 Synthesis

The synthesis of 6-nitroso-2-phenylimidazo[1,2-a]pyridine-3 carbaldehyde (C1) and (2-phenylimidazo[1,2-a]pyridin-3-yl)methanol (C2) was performed according to the procedure presented in Fig. 2 [14]:
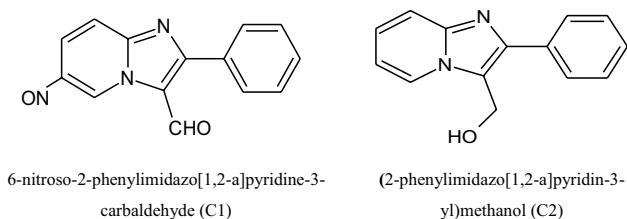

6-nitroso-2-phenylimidazo[1,2-a]pyridine-3-carbaldehyde (C1)

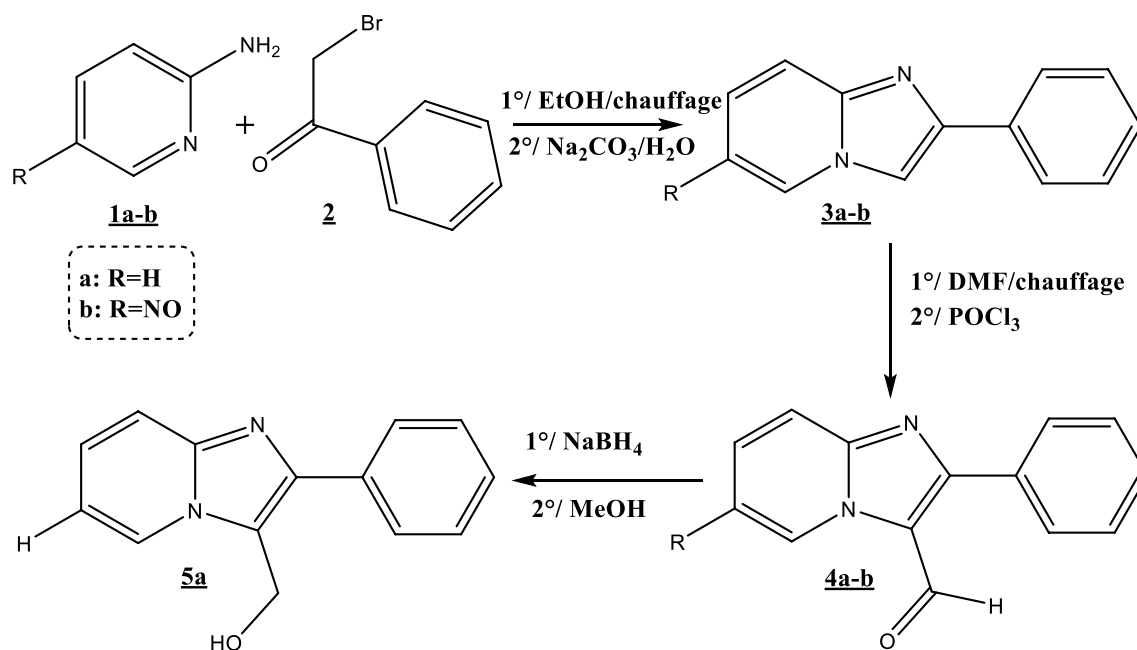(2-phenylimidazo[1,2-a]pyridin-3-yl)methanol (C2)

Fig. 1 The chemical structures of the studied inhibitors (C1) and (C2)

2.1.1 NPIPC: 6-Nitroso-2-phenylimidazo[1,2-a]pyridine-3 carbaldehyde (C1)

Yield 60%; RMN ^{1}H (300 MHz, CDCl3; TMS) δ (ppm): 7.5 (1H, td, H-Ar), 7.63 (3H, m, H-pyr, H-ar), 7.7 (2H, d, H-Ar, J = 7.75 Hz), 8.32 (1H, d, H-pyr, J = 8.76 Hz,), 8.83 (1H, s, H-pyr), 10.19 (1H, s, CHO).

2.1.2 PIPM: (2-Phenylimidazo[1,2-a]pyridin-3-yl)methanol (C2)

Yield 87%; RMN ^{1}H (DMSO-d6, 60 MHZ) δ (ppm): 8.56 (1H, dd, H5, J5–6 = 7.1HZ), 7.90 (3H, m, Har), 7.55 (4H, m, Har-Hpyr), 7.06 (1H, t, Hpyr J = 7.13 Hz), 5.00 (2H, s, CH$_2$), 3.30 (1H, s, OH).

2.2 Materials

The electrochemical experiments were performed on C-steel specimens with the following composition (in wt%): 0.21% C, 0.38% Si, 0.05% Mn, 0.05% S, 0.09% P, 0.01% Al, and balance Fe [15, 16]. Prior to each experiment, the specimens were pretreated by grinding with a series of emery papers (grades 400, 600, 800, 1000, 1200, and 1500), then washed with distilled water, degreased with acetone, and finally dried. 1.0 M HCl solution (Blank) was prepared by dilution of analytical grade HCl (37% w/w) with distilled water. The testing solutions consisted of 1.0 M HCl without and with (C1) and (C2) at the following concentrations $(1.0 \times 10^{-6}, 1.0 \times 10^{-5}, 1.0 \times 10^{-4},$ and 1.0×10^{-3} M). The

Fig. 2 Synthesis of the new compounds (C1) and (C2)

molecular properties have been studied using density functional theory (DFT) methods at B3LYP/6-31G (d,p) level of theory set with GAUSSIAN 09W program [17].

2.3 Electrochemical Measurements

Electrochemical potentiodynamic polarization (EPP) and impedance spectroscopy (EIS) experiments were performed in a conventional three-electrode cell using a potentiostat PGZ 100 driven by Volta Master software [12]. The working electrode (WE) consisted of Carbon steel specimen, Ag/AgCl used as a reference electrode, and platinum wire as the counter (auxiliary) electrode. The temperature of the solution was thermostatically controlled in a water bath. Prior to the electrochemical experiment, a stabilization period of 30 min was allowed, and this was proved to be sufficient to reach a steady-state open circuit potential. The polarization curves were recorded from -900 to -100 mV with scan rate of 1 mV s^{-1}. All experiments were repeated three times at the desired temperature (± 1 °C). In order to evaluate the corrosion kinetic parameters, a fitting by Stern–Geary equation was used. To do so [18, 19], the overall current density values, i, were considered as the sum of two contributions, anodic and cathodic current i_a and i_c, respectively. This was derived from the following equation:

$$i = i_a + i_c = i_{corr}\left\{\exp\left[b_a \times (E - E_{corr})\right] - \exp\left[b_c \times (E - E_{corr})\right]\right\}, \tag{1}$$

where i_{corr} is the corrosion current density (A cm^{-2}); b_a and b_c are the Tafel constants of anodic and cathodic reactions (V^{-1}), respectively.

These constants are linked to the Tafel slopes (V dec^{-1}) in logarithmic scale given by the following equation:

$$\beta = (\ln 10/b) = (2.303/b), \tag{2}$$

where β is a constant, and b is the Tafel slope.

The percentage inhibition efficiency ($\eta_{PP}\%$) obtained from potentiodynamic polarization measurements was calculated using the following equation [20–23]:

$$\eta_{PP}\% = \frac{I_{corr} - I'_{corr}}{I_{corr}} \times 100, \tag{3}$$

where $\eta_{PP}\%$ is the percentage inhibition efficiency obtained from the potentiodynamic polarization experiments, and I_{corr} and I'_{corr} represent the values of uninhibited and inhibited corrosion current densities, respectively.

The electrochemical impedance spectroscopy (EIS) spectra were recorded by applying an alternating current (AC) signal with a 10 mV amplitude and the applied frequency ranged from 100 KHz to 10 mHz at open circuit potential, with 10 points per decade. The inhibition efficiency$\eta_{imp}\%$ of the tested inhibitors C1 and C2 was calculated from the charge-transfer resistance values (R_{ct}) using the following equation [24, 25]:

$$\eta_{imp}\% = \frac{R_{ct} - R'_{ct}}{R_{ct}} \times 100, \tag{4}$$

where $\eta_{imp}\%$ is the percentage inhibition obtained from electrochemical impedance spectroscopy experiments, and R'_{ct} and R_{ct} are the charge-transfer resistance in the absence and presence of inhibitor, respectively.

2.4 Scanning Electron Microscopy (SEM)

The surface morphology of the carbon steel specimen was analyzed in the presence and absence of inhibitor at an optimum concentration using scanning electron microscope (SEM) (FEI quanta 200). SEM was used to characterize in greater details the surface morphology of steel at low magnifications (50×). The specimens were immersed in 1.0 M HCl for 6 h in the absence and presence of C1 and C2 inhibitors. After immersion, each specimen was rinsed with distilled water, and dried.

2.5 Computational Study

Quantum chemical computations were carried out using Gaussian 09 [26, 27] software package, at density functional theory (DFT) with the Beck's 3-parameter hybrid exchange functional (B3) combined together with Lee–Yang–Parr (B3LYP) and 6-31G (d,p) basis set [28] in gas and aqueous phase. DFT used in this study has become very popular, in terms of applicability and as an accurate method to investigate the electronic structure of molecules [29]. The most relevant descriptors of the molecule potential as corrosion inhibitors include HOMO and LUMO energy values, energy band gap (ΔE), molecular dipole moment (μ), electron affinity (A), ionization potential (I), electronegativity (χ), global hardness (η), softness (σ), the fraction of electron transferred (ΔN), electrophilicity index (ω), and Fukui functions. All these parameters were calculated using the DFT method and have been used to understand the properties and activity of the two studied inhibitors and to explain the experimental data obtained for the corrosion process.

3 Results and Discussion

3.1 Potentiodynamic Polarization Measurements

The polarization curves of C-steel in 1.0 M HCl solution with and without the presence of various concentrations of (C1) and (C2) inhibitors are shown in Fig. 3. Electrochemical corrosion kinetic parameters, such as corrosion potential
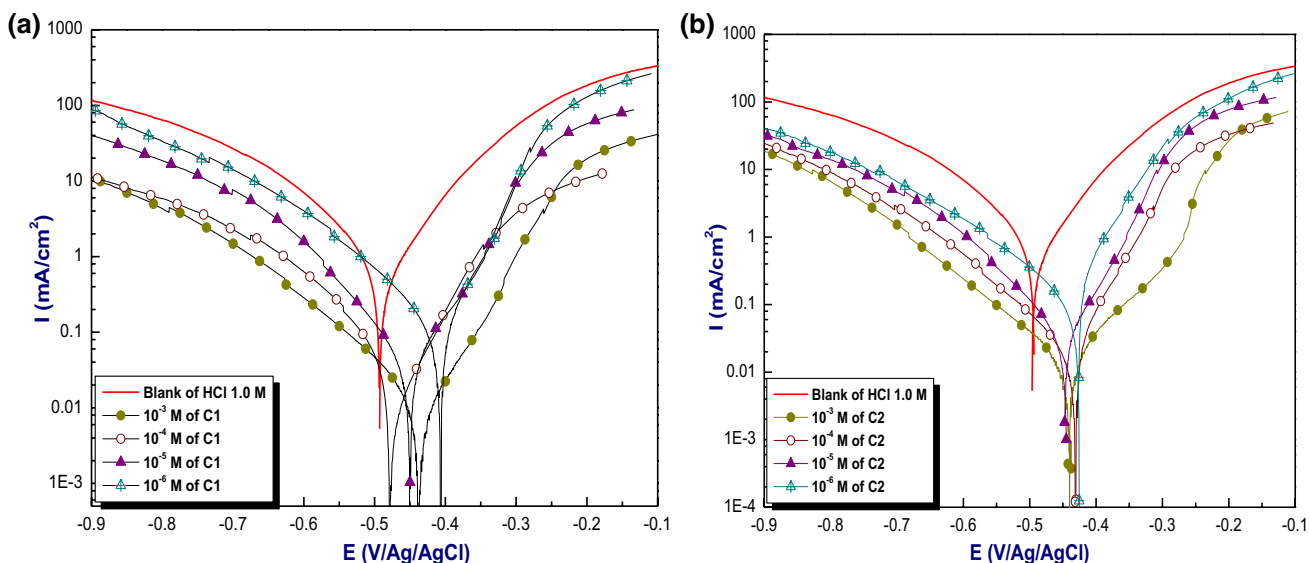
Fig. 3 Tafel polarization curves for the C-steel in 1.0 M HCl containing various concentrations of **a** C1 and **b** C2 inhibitors

(E_{corr}), corrosion current density (I_{corr}), and cathodic Tafel slopes (b_c) are presented in Table 1.

As it can be seen from these polarization results, the i_{corr} values decreased considerably with the increase of the inhibitor concentration [30]. For the uninhibited solution, the i_{corr} was 983 μA cm^{-2}, but in the presence of 1.0×10^{-3} M of C1 and C2, i_{corr} values decrease to 42 and 78 μA cm^{-2}, respectively, which indicates that the corrosion current markedly decreased in the presence of both inhibitors. This could be due to the adsorption process of the inhibitor by the most preferable sites onto surface of steel in acid solution [31].

Since the effect of the inhibitors on the cathodic Tafel slopes is negligible, this indicates that the adsorption of both inhibitors does not modify the mechanism of cathodic reaction [32]. Figure 3 shows the noticeable effect of C1 and C2 on the slope of anodic branches forming a protective film on the anodic sites. In addition, the potential shift towards more positive values corresponds to the dominant anodic inhibition mechanism of the tested compounds in acidic environment.

If the change in E_{corr} values in the presence of inhibitor is greater than 85 mV as compared to the E_{corr} value of blank, these compounds can be categorized as anodic or cathodic type [33]. However, if the change in E_{corr} values is less than 85 mV, then they act as mixed type inhibitors [34]. In our case, the maximum change for C1 is greater than 85 mV indicating that this compound acts as anodic inhibitor, while C2 act as mixed type with anodic predominance.

3.2 Electrochemical Impedance Spectroscopy Measurements

The Nyquist plots (Fig. 4) contain depressed semi-circles non-ideal with their center located under the real axis, and their size increases with the increase of the inhibitor concentration, indicating that the corrosion of metal is mainly

Table 1 Tafel polarization parameters for C-steel in 1.0 M HCl solution with and without the addition of various concentrations of C1 and C2 inhibitors

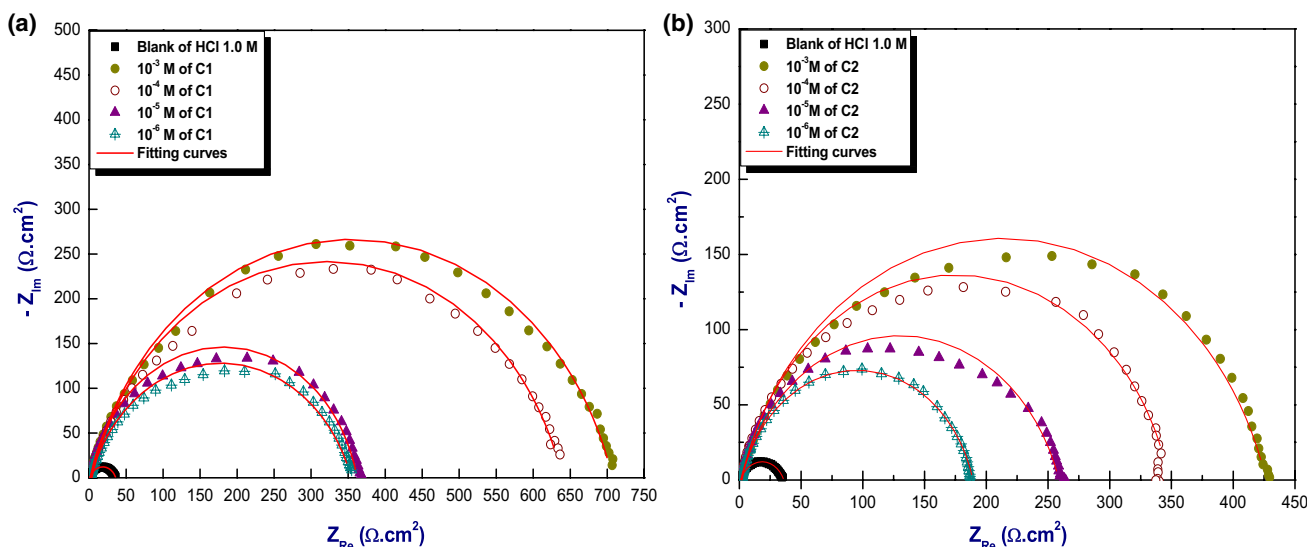| Medium	C (M)	E_{corr} (mV vs. Ag/AgCl)	i_{corr} (μA cm^{-2})	$-b_c$ (mV dec^{-1})	Θ	η_{PP} %
1.0 M HCl	0	−498	983	140	–	–
1.0 M HCl + C1	1.0×10^{-3}	−435	42	129	0.957	96
	1.0×10^{-4}	−477	49	145	0.950	95
	1.0×10^{-5}	−447	89	104	0.909	91
	1.0×10^{-6}	−405	91	130	0.907	91
1.0 M HCl + C2	1.0×10^{-3}	−436	78	129	0.92	92
	1.0×10^{-4}	−428	92	115	0.906	91
	1.0×10^{-5}	−443	127	110	0.870	87
	1.0×10^{-6}	−424	172	143	0.825	82

Fig. 4 Nyquist plots of C-steel in 1.0 M HCl solution containing various concentrations of **a** C1 and **b** C2 inhibitors at 298 K

related to the charge-transfer process [35, 36]. As seen from Fig. 5, the single peak obtained in Bode plots refers to the existence of one time constant. It can also be seen from Bode plots that the absolute impedance at low frequency increases with the increase of C1 and C2 concentrations forming a protective film on the steel surface [37]. Moreover, the more negative values of phase angle obtained from increasing the concentration of the inhibitors indicate a good inhibition effect on the corrosion of steel in 1.0 M HCl solution. This behavior could be due to the adsorption of more molecules on metal surface at higher concentration [38].

The obtained impedance data were fitted with the simulation EC-Lab V10.02 to the electrical equivalent circuit diagram shown in Fig. 6 [39]. A fitting circuit (Fig. 6) represented the charge-transfer resistance (R_{ct}) connected in parallel to the constant phase element (CPE), and both in a series connection with the solution resistance (R_s) [40]. CPE is used to replace the pure capacitance element in order to modeling the frequency dispersion generally related to different physical phenomena such as surface heterogeneity [41].

The impedance of CPE is given by the following equation:

$$Z_{CPE} = [Q(j\omega)^n]^{-1},\tag{5}$$

where Q is the frequency independent real constant, j is the imaginary number, $\omega = 2\pi f$ is the angular frequency (rad s^{-1}), f is the frequency of the applied signal, and n is the CPE exponent for whole number of $n = 1, 0, -1$. The calculated values of the double-layer capacitance (C_{dl}) derived from the CPE parameters were calculated according to the following equation [42]:

$$C_{dl} = (Q \times R_{ct}^{1-n})^{1/n}.\tag{6}$$

Excellent fit was obtained with this model of electrical circuit for all experimental data. The impedance parameters were calculated from the non-linear least square fit of the equivalent circuit and are given in Table 2.

As it can be seen from Table 2, the R_{ct} values increased and the C_{dl} values decreased with the increase of the inhibitor concentration. This variation can be interpreted by an increase of the double-layer thickness. The result can be attributed to the gradual replacement of water molecules with adsorbed inhibitors on the metal surface [43, 44]. The percent inhibition (η_{imp} %) was calculated according to the following equation:

$$\eta_{imp}\% = \frac{R'_{CT} - R_{CT}}{R'_{CT}} \times 100,\tag{7}$$

where R_{CT} and R'_{CT} are the charge-transfer resistance without and with inhibitor, respectively.

The percent inhibition of the C-steel in the presence of high concentration of C1 and C2 reached 95% and 92%, respectively. The better adsorption of C1 could be related to the strong reactivity of aldehyde (CHO) and nitroso (–N=O) functional at the groups metal/solution interfaces.

3.3 Adsorption Isotherm and Thermodynamic Parameters

To obtain information on the adsorption mode of C1 and C2 on the C-Steel surface, different adsorption isotherms were tested. The value of linear regression coefficient (R^2) was used as a guage in selecting the isotherm that best described the adsorption process [45]. The EIS data were tested using three adsorption isotherms, which included Temkin,
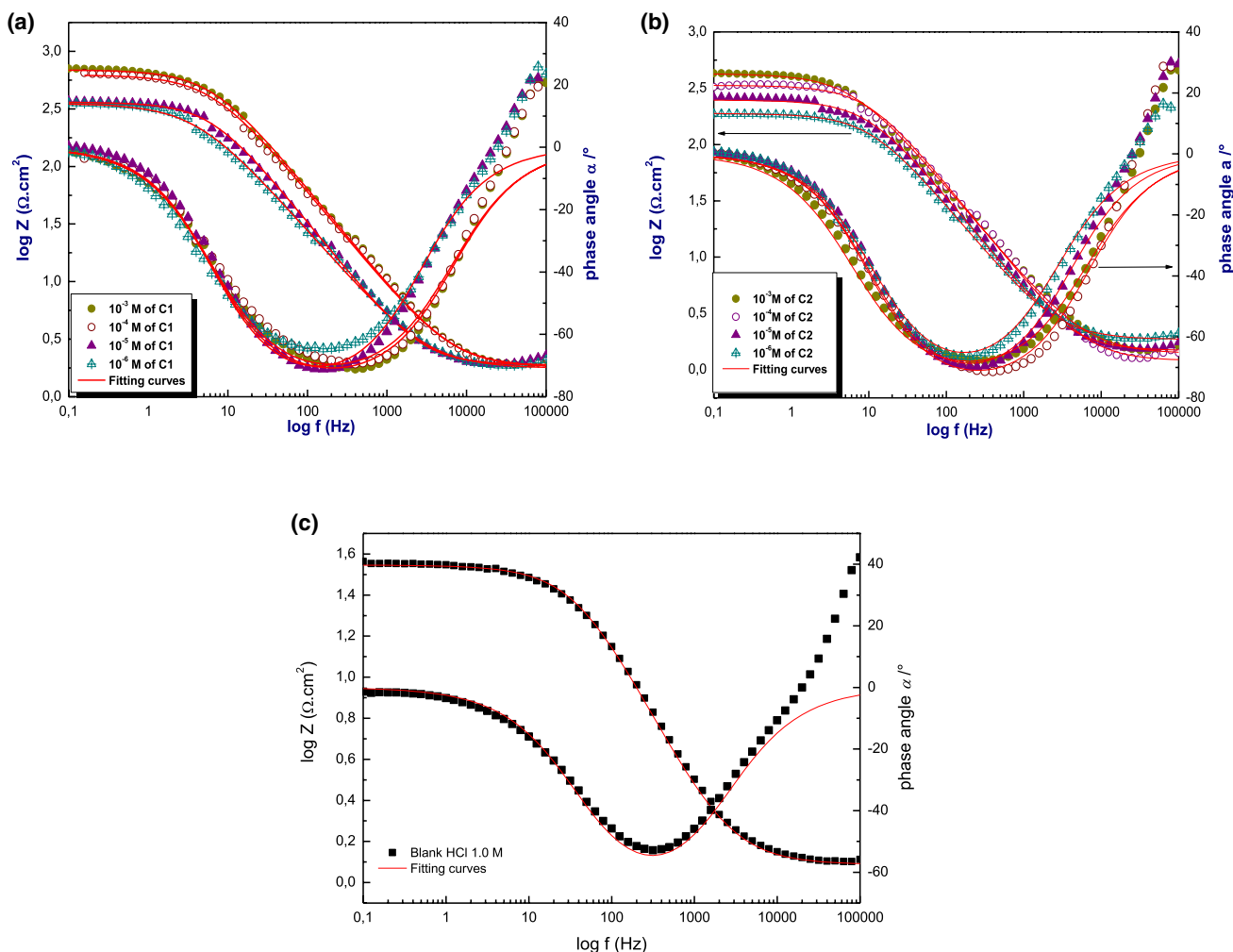
(a)

(b)

(c)

Fig. 5 Bode plots for C-steel in 1.0 M HCl solution containing various concentrations of **a** C1 and **b** C2 inhibitors, and **c** the blank
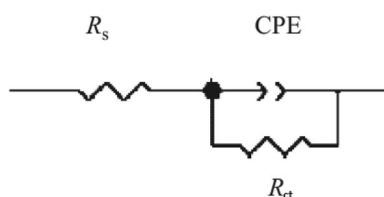

Fig. 6 Electrical equivalent circuit used for the modeling the steel/electrolyte system

Frumkin, and Langmuir models. The Langmuir adsorption isotherm model has best fitted the data for C1 and C2 and is described by the following equation [46]:

$$\frac{C_{\text{inh}}}{\theta} = C_{\text{inh}} + \frac{1}{K}, \tag{8}$$

where θ is the degree of surface coverage, C_{inh} is the inhibitor concentration, and K is the equilibrium constant of the adsorption/desorption process.

The choice of Langmuir isotherm over the other isotherms was based on the correlation coefficient (R^2) values where it was found to be closer to unity with the Langmuir isotherm. The plot of the linear fit of C_{inh}/θ vs. C_{inh} (Fig. 7) showed straight lines with an average regression coefficient and slope close to unity [46].

In order to attribute the adsorption process to either physisorption or chemisorption, the free energy of adsorption (ΔG_{ads}) was calculated for the Langmuir isotherm using Eq. 9 and illustrated in Table 3:

$$\Delta G_{\text{ads}} = -RT \ln (55.5 \, K), \tag{9}$$

where ΔG_{ads} is the standard free energy of adsorption, R is the gas constant, and T is the absolute temperature. The value of 55.5 is the concentration of water in solution in M.

Generally, if the absolute value of ΔG_{ads} is lower than 20 kJ mol^{-1}, the adsorption can occur through electrostatic forces involving weaker interactions between the inhibitor charged molecules and the charge of metal [47]. If the

Table 2 Impedance parameters for C-steel in 1.0 M HCl solution in the absence and presence of different concentrations of C1 and C2 at 298 K

| Medium	C (M)	R_s (Ω cm^2)	R_{ct} (Ω cm^2)	C_{dl} (μF cm^{-2})	n_{dl}	Q (μF S^{n-1})	Θ	η_{imp} %
1.0 M HCl	0	1.12 ± 0.2	34.7 ± 0.59	121	0.773 ± 0.02	419 ± 0.028	–	–
1.0 M HCl + C1	1.0×10^{-3}	2.2 ± 0.2	704.8 ± 0.4	37.11	0.824 ± 0.01	70.42 ± 0.4	0.95	95
	1.0×10^{-4}	1.8 ± 0.2	635.6 ± 0.4	39.55	0.827 ± 0.02	74.61 ± 0.6	0.945	94
	1.0×10^{-5}	1.88 ± 0.2	360 ± 0.4	69.37	0.868 ± 0.01	112.9 ± 0.15	0.903	90
	1.0×10^{-6}	1.76 ± 0.2	352.5 ± 0.4	108	0.799 ± 0.01	208 ± 0.26	0.901	90
1.0 M HCl + C2	1.0×10^{-3}	1.38 ± 0.2	425.2 ± 0.4	61.09	0.824 ± 0.01	116 ± 0.13	0.918	92
	1.0×10^{-4}	2.27 ± 0.2	345.8 ± 0.3	50.88	0.850 ± 0.02	93.04 ± 0.13	0.899	90
	1.0×10^{-5}	1.2 ± 0.2	257.7 ± 0.4	65.59	0.815 ± 0.01	139.3 ± 0.15	0.865	86
	1.0×10^{-6}	1.85 ± 0.2	187.3 ± 0.4	77.31	0.842 ± 0.01	150.5 ± 0.15	0.815	81
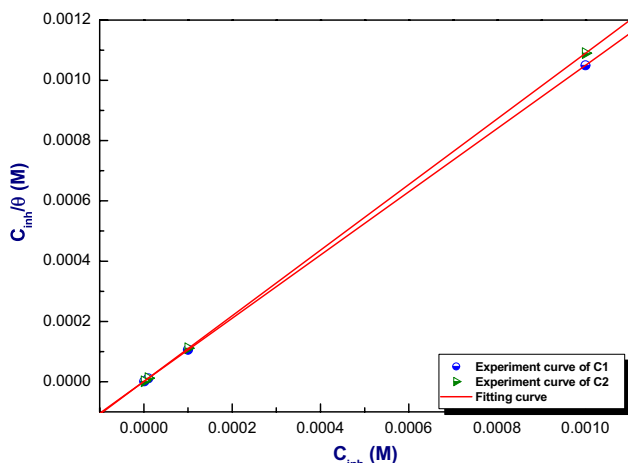
Fig. 7 Langmuir adsorption isotherm plots of C-steel in 1.0 M HCl solution containing C1 and C2

Table 3 Langmuir parameters representing the adsorption mechanism on C-steel surface obtained from EIS parameters at 298 K

Inhibitors	K (L mol^{-1})	ΔG^0_{ads} (KJ mol^{-1})
C1	25.37×10^5	− 46.48
C2	9.75×10^5	− 44.12

value of ΔG_{ads} becomes − 40 kJ mol^{-1} or more negative, then chemisorption would dominate [47]. The value of ΔG_{ads} at 298 K is found to be − 46.48 kJ mol^{-1} for C1 and − 44.12 kJ mol^{-1} for C2 (Table 3). It can be inferred from this result that both compounds show an active chemisorption towards the metal surface to form a coordinate chemical bond. However, chemisorption was the major contributor, while physical adsorption only slightly contributed to the adsorption mechanism judged from the decrease of R_{ct} with the increase in temperature [39].

3.4 Effect of Immersion Time

In order to investigate the inhibitors adsorption kinetics and to determine the time needed for C1 and C2 to reach their maximum inhibition efficiencies, electrochemical impedance spectroscopic measurements in 1.0 M HCl solution were performed in the absence and presence of 1.0×10^{-3} M tested compounds for different immersion times. The results are shown in Fig. 8 and Table 4.

Table 4 shows that η_{imp} % increases with the increase of immersion time reaching maximum values after 4-h immersion for both inhibitors (96% for C1 and 93% for C1). However, for prolonged immersion times (more than 4 h), the η_{imp} % slightly decreases and reaching about 94% for C1 and 91% for C2 after 12-h immersion time. Both tested molecules formed a compact film within an immersion time of 1 h and after 4 h this film started to detach from the electrode surface leading to a decrease in the inhibition efficiency. This is the result of the permeation of the electrolyte through the protective layer formed on the metal surface.

3.5 Effect of Temperature and Thermodynamic Parameters

The temperature can modify the interaction between the C-steel and the inhibitors in acidic medium [46]. In order to study the effect of temperature on the inhibition efficiencies of the imidazopyridine compounds, polarization and impedance experiments were conducted in the range of 298–328 K, in the absence and presence of 1.0×10^{-3} M of C1 and C2. The results showed that an increase in the temperature decreased very slightly the corrosion rate in the presence of the both inhibitors compared to the blank solution (Fig. 9) (Table 5). This indicates that the dissolution of metal is mainly controlled by chemical adsorption of C1 and C2 which involves strong interactions between the studied inhibitors and metal surface.
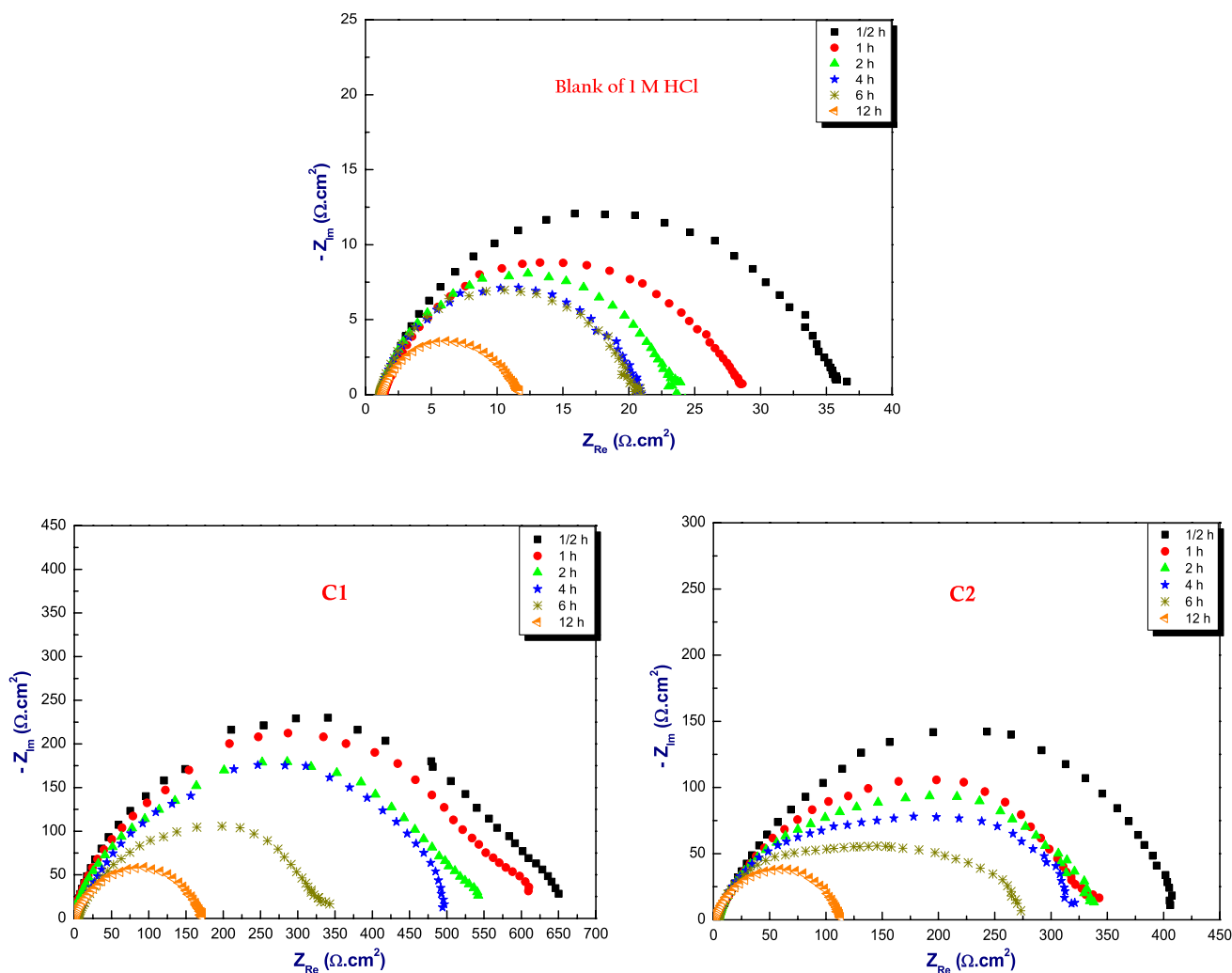
Fig. 8 Nyquist diagrams of C-steel in 1.0 M HCl with and without 1.0×10^{-3} M C1 and C2 at 25 °C for different immersion times

In order to estimate the activation energy (E_a), the enthalpy of activation (ΔH^*), and the entropy of activation (ΔS^*) for the corrosion reaction of C-steel in the absence and presence of C1 and C2, the Arrhenius equation was used:

$$\ln I_{corr} = -\frac{E_a}{RT}, \tag{10}$$

where E_a is the apparent effective activation energy, T is the absolute temperature, and R is the gas constant.

The values of apparent activation energy are listed in Table 6. An alternative formulation of the Arrhenius equation is the thermodynamic formulation of the transition state theory:

$$\ln \frac{I_{corr}}{T} = \left(\frac{RT}{N \times h} \right) \exp \left(\frac{\Delta S^*}{R} \right) \exp \left(\frac{-\Delta H^*}{RT} \right), \tag{11}$$

where N is the Avogadro's number, h is the Plank's constant, ΔH^* is the enthalpy of activation, and ΔS^* is the entropy of activation.

The activation parameters of for C-steel in 1.0 M HCl acid solution in the absence and presence of C1 and C2 were obtained from linear square fits of $\ln I_{corr}$ vs. $1000/T$ (Fig. 10). The values of ΔH^* and ΔS^* were obtained from linear square fits of $\ln I_{corr}/T$ vs. $1000/T$ (Fig. 11).

Figure 10 shows the Arrhenius plots in the absence and presence of 1.0×10^{-3} M of imidazopyridine inhibitors. The corresponding values of E_a are given in Table 6 and indicate that values of E_a obtained in solutions containing C1 and C2 are higher than those in the blank. The higher values of the apparent activation energy obtained in the presence of these compounds suggest that of C1 and C2 could be physisorbed on the C-steel surface [48]. The ΔH^* values for dissolution reaction of C-steel in 1.0 M HCl

Table 4 Electrochemical impedance parameters of the C-steel in 1.0 M HCl solution with and without 1.0×10^{-3} M C1 and C2 at 25 °C for different immersion times

| Medium	Time (h)	R_s (Ω cm^2)	R_{ct} (Ω cm^2)	C_{dl} (μF cm^{-2})	n_{dl}	Q (μF S^{n-1})	η_{imp} %
1.0 M HCl	½	1.28±0.2	33.84±0.5	117.7	0.815±0.02	327.0±0.5	–
	1	1.3±0.3	26.62±0.4	140.7	0.779±0.01	482.0±0.1	–
	2	1.12±0.3	22.11±0.5	224.4	0.821±0.02	579.0±0.1	–
	4	1.03±0.2	19.51±0.4	287.8	0.827±0.03	705.5±0.2	–
	6	1.02±0.2	19.17±0.4	345.9	0.828±0.02	818.5±0.2	–
	12	1.28±0.3	10.21±0.5	142.5	0.807±0.01	501.1±0.3	–
1.0 M HCl + 1.0×10^{-3} M C1	½	0.77±0.02	643.5±0.6	30.28	0.780±0.01	71.91±0.5	95
	1	0.83±0.02	600.7±0.4	30.86	0.779±0.02	74.47±0.6	95
	2	1.3±0.03	540.0±0.7	35.76	0.755±0.01	93.73±0.9	96
	4	4.4±0.2	515.0±0.4	66.44	0.745±0.01	157.0±0.1	96
	6	1.75±0.2	374.4±0.5	52.89	0.755±0.03	138.2±1.7	95
	12	1.14±0.2	171.6±0.4	49.71	0.754±0.02	160.4±0.5	94
1.0 M HCl + 1.0×10^{-3} M C2	½	3.7±0.2	422.2±0.5	75.08	0.731±0.02	190.0±0.3	92
	1	4.06±0.2	336.6±0.6	67.6	0.720±0.01	194.9±0.2	92
	2	3.89±0.2	326.9±0.4	59.38	0.714±0.03	182.9±0.2	93
	4	3.7±0.2	299.8±0.3	61.33	0.700±0.01	202.9±0.4	93
	6	3.6±0.3	225.9±0.3	52.14	0.692±0.01	204.5±0.3	91
	12	1.29±0.2	112.9±0.4	65.52	0.751±0.03	222.0±1.1	91
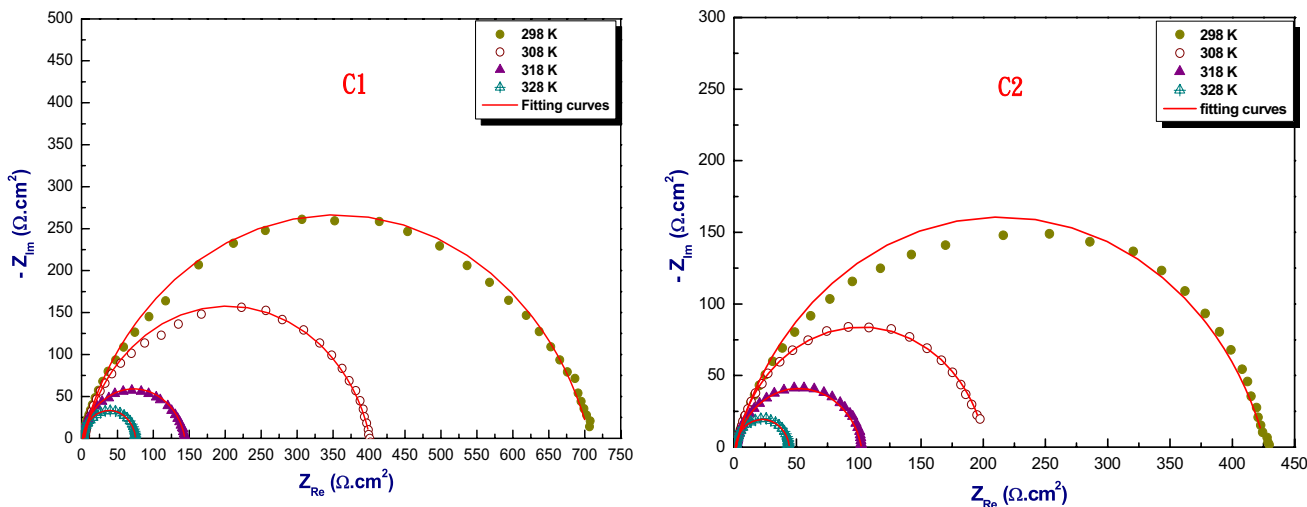
Fig. 9 Nyquist plots of C-steel in 1.0 M hydrochloric acid, in the absence and presence of 1.0×10^{-3} M of C1 and C2 at different temperatures

solution in the presence of C1 and C2 are higher than that in their absence. However, the positive signs of ΔH^* values reveal the endothermic nature of the C-steel dissolution process suggesting that is difficult with inhibitors. The negative values of entropy ΔS^* show that the formation of activated complex at the rate-controlled step represents an association step being more ordered [49].

3.6 Scanning Electron Microscopy (SEM)

The surface morphology of C-steel before and after immersion in 1.0 M hydrochloric acid in the absence and presence of 1.0×10^{-3} M of C1 and C2 was determined by SEM and is shown in Fig. 12. The electron micrographs reveal a smooth surface in absence of any treatment Fig. 12a; however, after an immersion in 1.0 M HCl solution for 6 h, the surface

Table 5 The electrochemical impedance parameters of C-steel in 1.0 M hydrochloric acid solution in the absence and presence of 1.0×10^{-3} M of C1 and C2 at different temperatures

Medium	T (K)	R_s (Ω cm^2)	R_{ct} (Ω cm^2)	C_{dl} (μF cm^{-2})	n_{dl}	Q (μF S^{n-1})	η_{imp} %
1.0 M HCl (Blank)	298	1.12 ± 0.29	34.7 ± 0.59	121	0.773 ± 0.02	419 ± 0.028	–
	308	1.8 ± 0.27	20.86 ± 0.46	102	0.766 ± 0.02	431 ± 0.05	–
	318	2.1 ± 0.2	11.35 ± 0.4	139	0.722 ± 0.02	837 ± 0.04	–
	328	1.16 ± 0.28	6.87 ± 0.4	158	0.797 ± 0.03	629 ± 0.13	–
1.0 M HCl + 1.0×10^{-3} M of C1	298	2.2 ± 0.2	704.8 ± 0.4	37.11	0.824 ± 0.01	70.42 ± 0.4	95
	308	4.31 ± 0.27	397 ± 0.5	65.29	0.854 ± 0.01	111 ± 0.1	95
	318	1.22 ± 0.2	142.6 ± 0.4	116	0.880 ± 0.01	189.4 ± 0.3	92
	328	1.8 ± 0.19	73.48 ± 0.4	387	0.935 ± 0.01	499 ± 0.25	90
1.0 M HCl + 1.0×10^{-3} M of C2	298	1.38 ± 0.2	425.2 ± 0.4	61.09	0.824 ± 0.01	116 ± 0.13	92
	308	1.89 ± 0.18	200.3 ± 0.6	71.7	0.887 ± 0.02	892 ± 0.1	90
	318	1.57 ± 0.2	100.6 ± 0.4	63.58	0.870 ± 0.02	122.5 ± 0.19	89
	328	0.97 ± 0.1	43.44 ± 0.4	73.8	0.926 ± 0.01	951.6 ± 0.6	84

Table 6 Activation parameters, E_a, ΔH^*, and ΔS^* of the dissolution of C-steel in 1.0 M HCl solution in the absence and presence of 1.0×10^{-3} M C1 and C2

Medium	E_a (kJ mol^{-1})	ΔH^* (kJ mol^{-1})	ΔS^* (kJ mol^{-1}k^{-1})
1.0 M HCl (Blank)	21	18.5	-126
1.0 M HCl + 1.0×10^{-3} M of C1	39.56	36.96	-90.33
1.0 M HCl + 1.0×10^{-3} M of C2	36	33.47	-96.62

was strongly damaged owing to corrosion in the absence of the inhibitors (Fig. 12b), but in the presence of the inhibitors (Fig. 12c, d) there was less damage on the surface. The surface morphology of steel in the presence of C1 and C2 showed large smooth area, free of corrosion products, and revealed the formation of a protective layer on the C-steel surface [16].

3.7 Quantum Chemical Calculations

Quantum chemistry has been largely applied to understand the complex mechanism of corrosion inhibition between organic molecules and metal surface [50]. Quantum descriptor calculations were performed using Density Functional
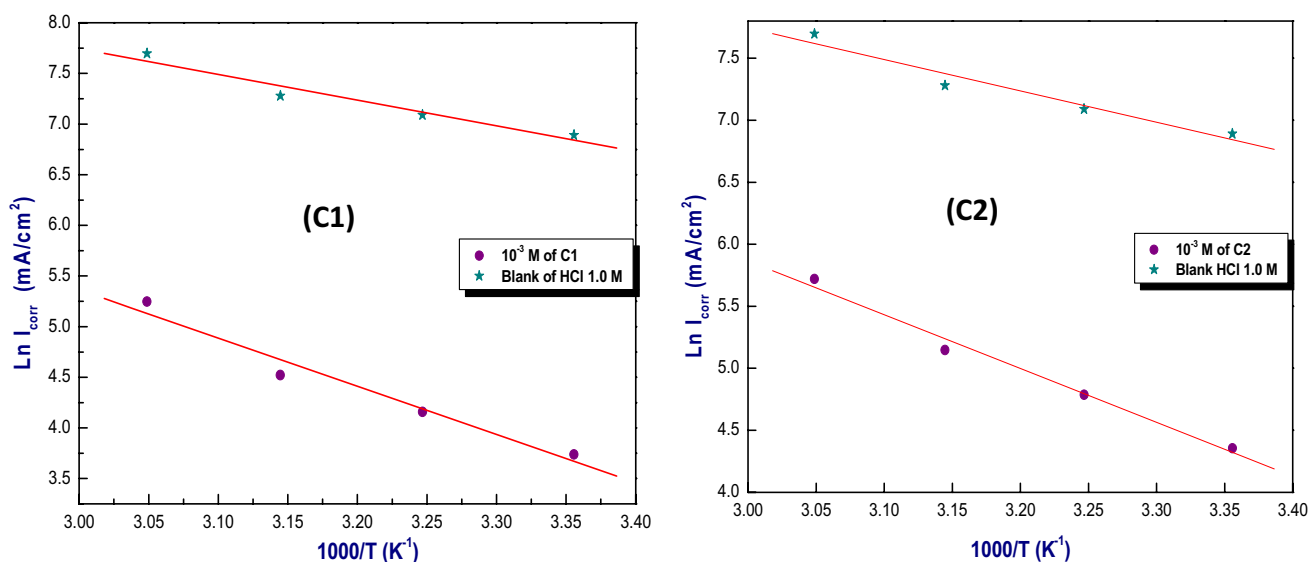

Fig. 10 Arrhenius plots (ln I_{corr} vs. 1000/T) of C-steel in 1.0 M HCl solution with and without 1.0×10^{-3} M of C1 and C2
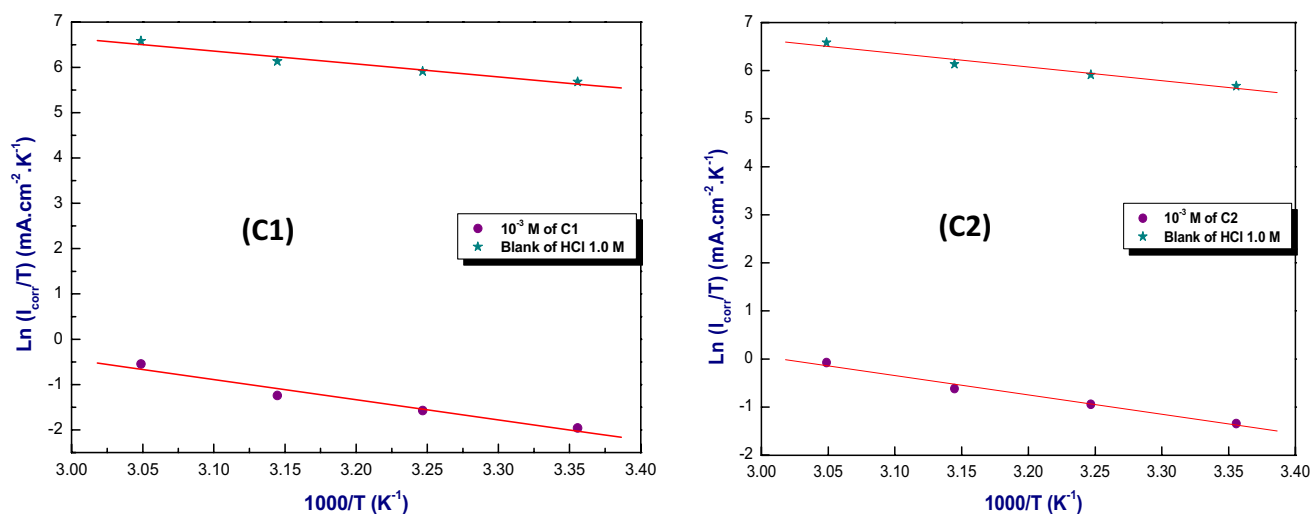
Fig. 11 Arrhenius plots (ln I_{corr}/T vs. $1000/T$) of C-steel in 1.0 M HCl solution with and without 1.0×10^{-3} M of C1 and C2
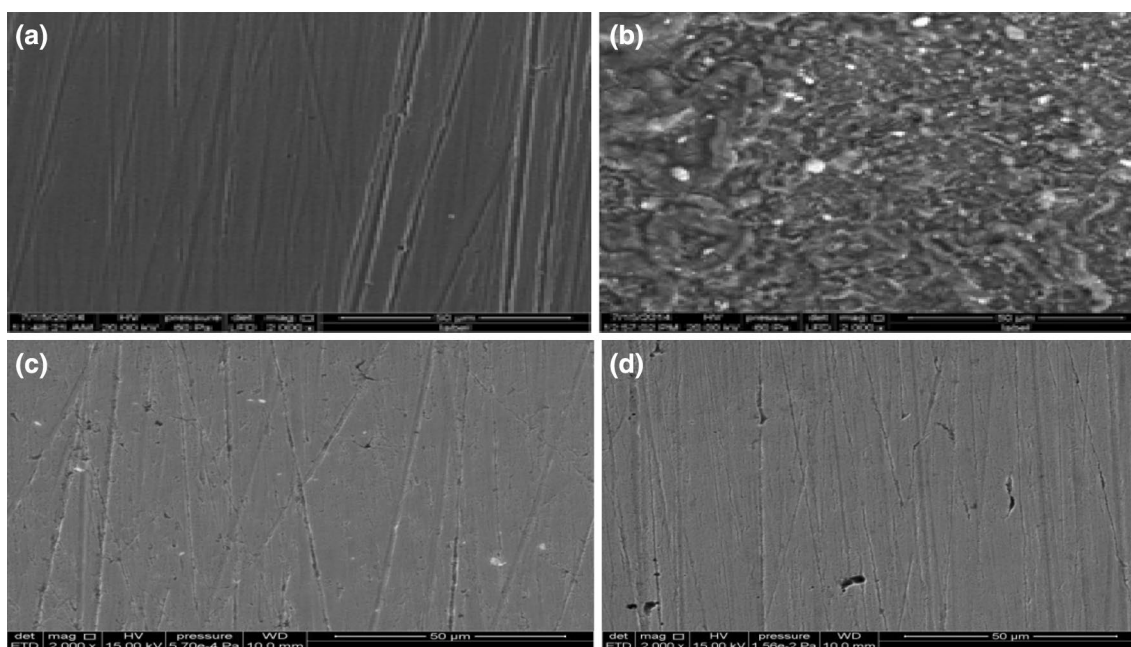

Fig. 12 SEM of carbon steel ($\times 50$ magnifications): **a** polished, **b** immersed for 6 h in 1.0 M HCl; **c** immersed for 6 h in 1.0 M HCl $+ 1.0 \times 10^{-3}$ M C1, **d** immersed for 6 h in 1.0 M HCl $+ 1.0 \times 10^{-3}$ M C2

Theory (DFT), B3LYP with 6-31G(d,p). The optimized geometries of the studied inhibitors and their frontier molecular orbitals (HOMO and LUMO) are presented in Fig. 13. The Fukui functions have also been modeled using a Mulliken populations analysis in order to establish the most active and reactive sites of the tested molecules. It can be seen that C1 and C2 have a similar HOMO distribution which are all mainly distributed almost of the whole molecule. The LUMO electronic density is saturated around imidazopyridine rings and nitroso group in C1 and distributed

on the entire molecule in C2 (Fig. 13). Electrostatic potential surfaces (ESP) maps give an indication of the net electrostatic effect of molecule produced at that point by the total charge distribution [51]. The different values of the electrostatic potential are shown with different colors, red color represents the regions of the most negative electrostatic potential, and the most positive electrostatic potential is indicated by a blue color, while the green color represents the region of zero potential [51]. The electrophilic active regions are localized around the oxygen and nitrogen
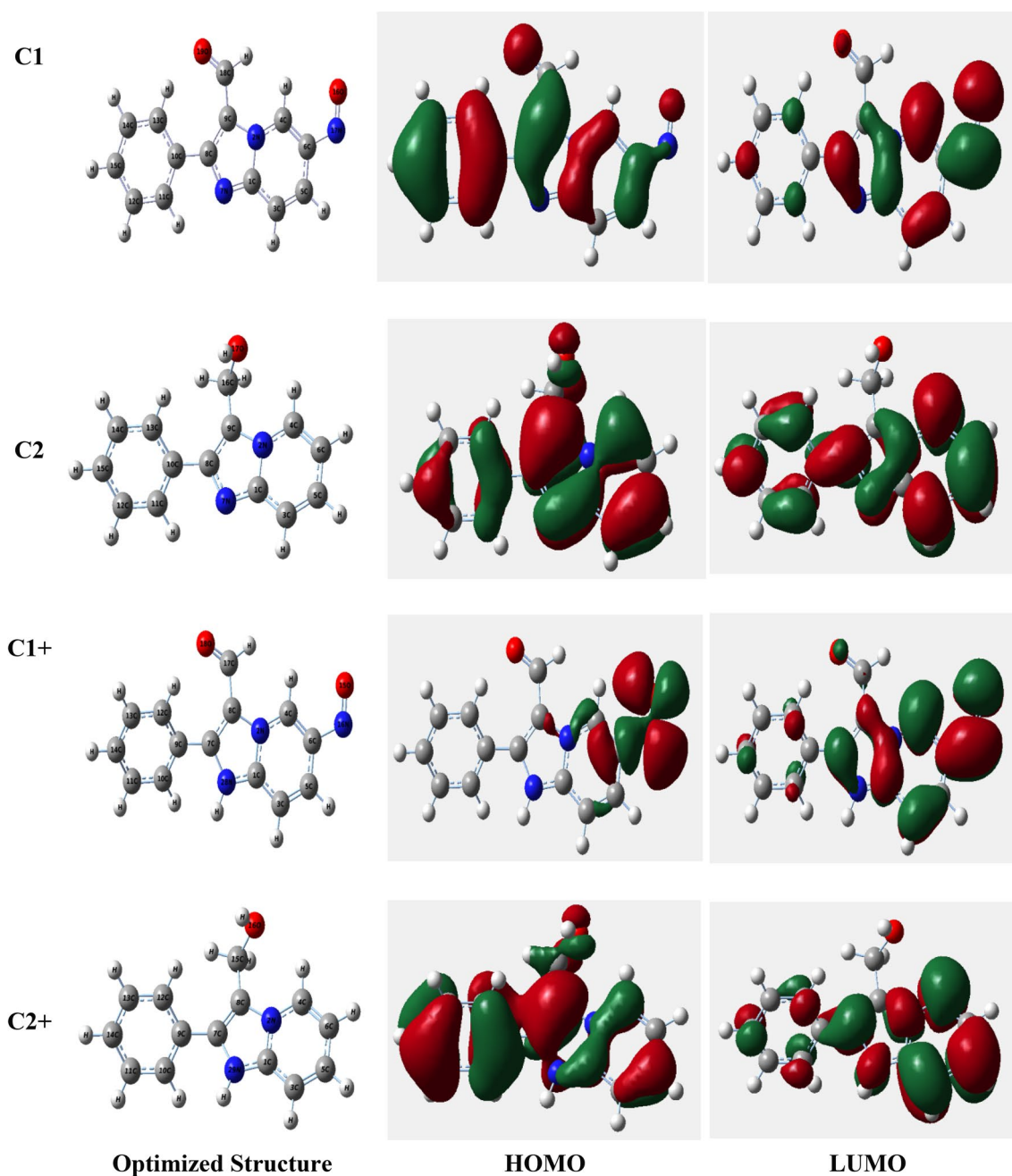
Optimized Structure **HOMO** **LUMO**

Fig. 13 Optimized structures, HOMO, LUMO for the studied compounds in *neutral* and *protonated forms* (B3LYP/6-31G (d,p))

atoms (especially O16, O19, and N7 atoms). As for the ESP contours presented in Fig. 14, the red lines are mainly concentrated around the same atoms and are possible sites for electrophilic attack.

The quantum parameters obtained from this study, such as E_{HOMO}, E_{LUMO}, energy gap (ΔE_{gap}), the dipole moment (μ), total energy (TE), absolute hardness (η), absolute electronegativity, (χ), and softness (σ), were calculated and are shown in Table 7. The frontier orbitals such as the highest occupied molecular orbital energy (E_{HOMO}) and the lowest

unoccupied molecular orbital energy (E_{LUMO}) are very important quantum chemical parameters to describe the chemical reactivity and ability of molecules to adsorb on the metal surface. The HOMO is the highest energy orbital containing electrons and act as an electron donor [52]. The LUMO is the innermost (lowest energy) orbital that could act as the electron acceptor [52]. The higher value of the HOMO energy indicates the tendency of a molecule (inhibitor) to donate electrons to appropriate acceptors such as 3d orbital of Fe atom; on the other hand, the value of LUMO

Fig. 14 Electrostatic potential surface ESP maps and contours of investigated inhibitors (C1 and C2) with B3LYP/6-31G (d,p) basis
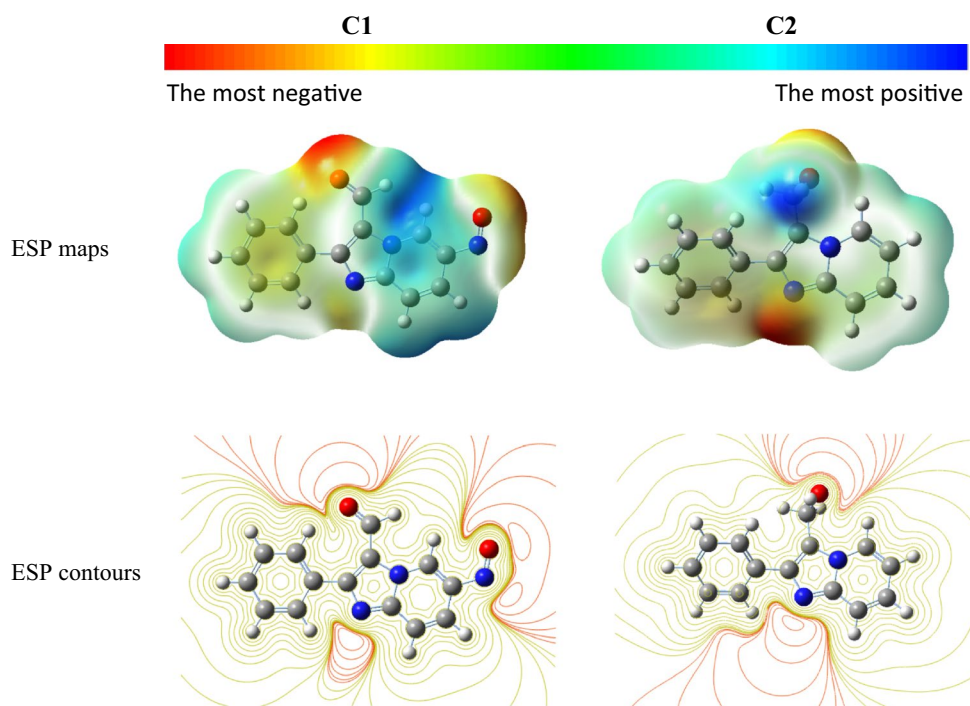

Table 7 Calculated quantum chemical parameters for non-protonated and protonated molecules of C1 and C2 obtained with the DFT at B3LYP/6–31 (d,p) level in gas and aqueous phases

Parameter	Phase	C1	C2	C1+	C2+
E_{HOMO} (eV)	G	− 6.4606	− 5.6483	− 10.0733	− 9.8812
	A	− 6.4560	− 5.7308	− 7.0212	− 6.7472
E_{LUMO} (eV)	G	− 3.2893	− 1.0563	− 6.9129	− 5.4119
	A	− 3.2197	− 1.1167	− 3.7462	− 2.0438
ΔE_{gap} (eV)	G	3.1712	4.5920	3.1604	4.4692
	A	3.2363	4.6140	3.2749	4.7033
η (eV)	G	1.5856	2.2960	1.5802	2.2346
	A	1.6181	2.3070	1.6374	2.3516
σ (eV^{-1})	G	0.6306	0.4355	0.6328	0.4474
	A	0.6179	0.4334	0.6106	0.4252
χ (eV)	G	4.8750	3.3523	8.4931	7.6465
	A	4.8378	3.4238	5.3837	4.3955
ω	G	7.4940	2.4473	22.8241	13.0826
	A	7.2320	2.5406	8.8504	4.1079
ε	G	0.1334	0.4085	0.0438	0.0764
	A	0.1382	0.3936	0.1129	0.2434
ΔN	G	0.6700	0.7943	− 0.4724	− 0.1446
	A	0.6680	0.77506	0.4935	0.5537
μ (D)	G	2.6310	1.4200	5.9861	3.9465
	A	3.2353	2.3846	8.2103	5.5064
Total energy	G	− 23226.4820	− 19741.1759	− 23236.6263	− 19752.0903
	A	− 23226.7982	− 19741.4668	− 23238.8171	− 19753.9988

G gas phase, *A* aqueous phase

energy indicates the capability of the molecule to accept electrons [53]. The smaller value of ΔE_{gap} of the inhibitors facilitates the adsorption of the molecule and thus will cause higher inhibition efficiency, because the energy to remove an electron from the last occupied orbital will be low [54]. A hard (High η) molecule has a large ΔE_{gap} and a soft molecule

(High σ) is associated with a small ΔE_{gap} [55]. Therefore, higher σ is related to the high reactivity of molecules [56]. The softness (σ) is the inverse of the hardness $= 1/\eta$.

A high value for the fraction of electron transferred is related to the high inhibition efficiency. The expression (ΔN) is explained by the simple movement of electrons from donor to the acceptor molecule [56]. According to Lukovits's study [57], if $\Delta N < 3.6$, the inhibition efficiency enhances with increasing electron donating ability at the metal surface. To calculate ΔN, the theoretical values of $\chi_{Fe} = 7$ eV and $\eta_{Fe} = 0$ eV are used in the following equation:

$$\Delta N = \frac{\chi_{Fe} - \chi_{inh}}{2(\chi_{Fe} + \chi_{inh})}, \tag{12}$$

where χ_{Fe} and χ_{inh} are the absolute electronegativity of metal and inhibitor molecules, respectively. χ_{Fe} and χ_{inh} are the absolute hardness of metal and the inhibitor molecule, respectively.

The electrophilicity (ω), nucleophilicity (ε), and total energy are chemical reactivity descriptors that provide the capacity of the molecule to receive and release electrons. In this case, C1 is the strongest electrophile, while C2 is the strongest nucleophile. Dipole moment (μ) is the measure of polarity of a polar covalent bond. It is defined as the product of charge on the atoms and the distance between the two bonded atoms [58]. A molecule with high value of dipole moment (μ) is explained by its higher polarizability and good effective surface area and therefore it would be a better corrosion inhibitor [59]. The highest value of the dipole moment (≈ 3 D) was shown for C1, which has the highest reactivity towards tested steel surface [60]. The calculated quantum chemical parameters in the presence of water as well as in the gas phase are gathered in Table 7. It was shown that the calculated quantum chemical parameters for non-protonated forms of imidazopyridine derivatives in the presence of a solvent (water) as well as in the gas phase do not exhibit important differences (Table 7). From the computed results in gas and aqueous phases, a high increase is shown for dipole moment (μ) in solution, which is probably a result of the polarization of the inhibitor molecules by the solvent, leading to an increase in the charge separation in the molecules [61].

The presence of nitrogen heteroatoms in the molecules of imidazopyridine derivatives suggests high tendency towards protonation in acidic solution (in our case 1.0 M HCl) [52]. Therefore, it is important to investigate the protonated forms of the imidazopyridine inhibitors. It is clear from the optimized structures of the investigated molecules in neutral forms that there are multiple possible sites for protonation. All the possible active sites for the protonation of optimization of structures were studied and it was found that the most probable one for C1 and C2 with lowest energy is the nitrogen atom (N7) with the highest negative charge.

The extent of protonation is provided by the proton affinity (PA) of the inhibitor which is estimated using the equation [60]:

$$PA = E_{prot} + E_{H_2O} - \left(E_{non\text{-}prot} + E_{H^+}\right), \tag{13}$$

where $E_{non\text{-}prot}$ and E_{prot} are the energies of the non-protonated and protonated inhibitors, respectively. E_{H^+} is the energy of H$^+$ ion and was calculated as follows:

$$E_{H^+} = E\left(H_3O^+\right) - E(H_2O). \tag{14}$$

In order to select the most favorable one, optimization of all possible structures with different active centers for protonation was carried out and it was found that the most probable one with lowest energy upon protonation was the N atom with the highest negative charge [62]. A high value of PA indicates that the molecule has a high tendency to be protonated [63]. The calculated PA values (kcal mol^{-1}) for C1 is 56.268 and 38.511 for C2, which indicates that C1 has the highest tendency for protonation in acidic media.

The quantum chemical calculation parameters such as EHOMO, ELUMO, ΔE, χ, σ, η, and ΔN derived for protonated form of C1 and C2 using 6-31G basic set are listed in Table 7. Similar to neutral form of the inhibitors, the lower value of ΔE for C1 compared to C2 indicates that C1 is more reactive and better corrosion inhibitor than C2. The values of global softness (σ) and hardness (η) also imply that C1 is a superior corrosion inhibitor compared to C2. This result validated our experimental finding that C1 is a superior corrosion inhibitor compared to C2 inhibitor. It was shown from the calculations that the highest coefficient in the HOMO level could be represented as a localization of charge density on N atom and delocalization of the π-charge on the ring moiety (N–C=N)$\rightarrow$ N$_{...}^-$C$_{...}$N which assists to greater extent in giving up its π electron density to the metal [64]. E_{HOMO} for the non-protonated forms was higher than for the protonated forms, which indicate that the protonation process decreases the electron donating ability of the tested inhibitors (Table 7). The solvent effect produced small changes in the calculated quantum chemical parameters of the tested compounds. However, a slight increase is shown for dipole moment values, due to molecular polarization generated by the effect of solvent molecules interaction [65].

The Fukui indices for some atoms of studied molecules which present the most active sites have been calculated in gaseous and aqueous phases (Table 8). Fukui functions are a measurement of local reactivity as well as indicative of local nucleophilic or electrophilic feature in the molecules [66]. It can be seen from Table 8 that the calculated values of f_k^+ for C1 are mostly localized on O16, N17, O19, and C1. On the other hand, O16, N17, C4, O19, and N7 are the most susceptible sites for the electrophilic attacks as they present the highest values of f_k^-. For C2 the largest values of

Table 8 Pertinent natural populations and Fukui functions of M1, M2, and M2 calculated at B3LYP/6-31G in gaseous (G) and aqueous phases (A)

Inhibitor	Atom k	Phase	P(N)	P(N+1)	P(N−1)	f_k^+	f_k^-
C1	9 C	G	0.2281	0.3232	0.2134	0.0950	0.0147
		A	0.2341	0.3695	0.2073	0.1354	0.0267
	16 O	G	−0.2762	−0.2107	−0.4568	0.0654	0.1806
		A	−0.2966	−0.2568	−0.5145	0.0397	0.2179
	19 O	G	−0.3568	−0.2968	−0.3999	0.0600	0.0431
		A	−0.4063	−0.3446	−0.4271	0.0617	0.0207
	7 N	G	−0.5511	−0.4982	−0.5926	0.0529	0.0414
		A	−0.5914	−0.5153	−0.6188	0.0760	0.0274
	1 C	G	0.5293	0.5675	0.5062	0.0382	0.0231
		A	0.5441	0.6066	0.5054	0.0625	0.0387
	17 N	G	−0.0399	0.0022	−0.2093	0.0422	0.1694
		A	−0.0556	−0.0254	−0.2733	0.0302	0.2176
	4 C	G	0.1560	0.1962	0.0461	0.0401	0.1098
		A	0.1812	0.2614	0.0442	0.0801	0.1369
C2	9 C	G	0.2307	0.3387	0.2137	0.1079	0.0170
		A	0.2346	0.3707	0.2033	0.1360	0.0313
	7 N	G	−0.5694	−0.4883	−0.6140	0.0811	0.0445
		A	−0.6181	−0.5272	−0.6660	0.0908	0.0479
	4 C	G	0.1118	0.1645	0.0261	0.0527	0.0856
		A	0.1107	0.1937	−0.0184	0.0829	0.1292
	5 C	G	−0.0771	−0.0313	−0.0934	0.0458	0.0163
		A	−0.0877	−0.0230	−0.1355	0.0646	0.0477
	1 C	G	0.5044	0.5485	0.4927	0.0441	0.0116
		A	0.5035	0.5713	0.4740	0.0678	0.0295
	3 C	G	−0.1312	−0.1091	−0.1950	0.0220	0.0638
		A	−0.1497	−0.1065	−0.2484	0.0432	0.0986

f_k^+ are located on the C9, N7, C4, C5, and C1 atoms, which further suggest that these atoms are responsible for forming a back bond by the acceptance of electron from the C-steel surface. However, the value of f_k^- is highest on C4, C3, N7, C15, and C5. The results also show that O16, O19, and N7 atoms are suitable sites to undergo both nucleophilic and electrophilic attacks for C1 which are more responsible for donor–acceptor interactions and thus facilitate the adsorption of the inhibitor on the metal surface.

4 Conclusion

Both studied compounds acted as good corrosion inhibitors for C-steel in 1.0 M hydrochloric acid solution and the inhibition efficiency (%) increased with increasing the inhibitor concentration to reach a maximum value of 96% for C1 and 92% for C2 at 1.0×10^{-3} M. The adsorption of the both organic molecules on the metal surface follows Langmuir adsorption isotherm. Potentiodynamic polarization study revealed that C1 and C2 acted as mixed type inhibitors with predominantly cathodic. EIS results showed that the imidazopyridine molecules inhibit carbon steel corrosion by their adsorption at the metal/acid interface due to an increase in thickness of the electrical double layer. SEM analyses further confirmed the protecting ability of the inhibitors molecules. The inhibitors adsorption on the metal surface is mixed type mechanism: physical adsorption resulting from the intermolecular force between the charged centers of molecules and the metal surface, which is relevant to the dipole of the inhibitors, and chemical adsorption resulting from the donation of π electron of imidazopyridine moiety and electron pairs of heteroatoms to the metal. The theoretical study using DFT calculations gave a good overview on the reactivity of the tested inhibitors towards C-steel and was in good agreement with the experimental results.

Compliance with Ethical Standards

References

1. Afia L, Lgaz H, Zougagh M, Belkhaouda M, Jodeh S, Algarra M (2016) Kaempferol as a corrosion inhibitor on mild steel in HCl Kaempferol as a corrosion inhibitor on mild steel in HCl. Appl J Envir Eng Sci 2(2):42–55

2. Elmsellem H, Basbas N, Chetouani A, Aouniti A, Radi S, Messali M, Hammouti B (2014) Quantum chemical studies and corrosion inhibitive properties of mild steel by some pyridine derivatives in 1 N HCl solution. Port Electrochim Acta 32(2):77–108

3. Karzazi Y, Belghiti ME, El-Hajjaji F, Boudra S, Hammouti B (2016) Density functional theory modeling and monte carlo simulation assessment of inhibition performance of two quinoxaline derivatives for steel corrosion. J Mater Environ Sci 7(11):4011–4023

4. Li W, He Q, Pei C, Hou B (2007) Experimental and theoretical investigation of the adsorption behaviour of new triazole derivatives as inhibitors for mild steel corrosion in acid media. Electrochim Acta 52(22):6386–6394

5. Verma C, Quraishi MA, Ebenso EE, Obot IB, El Assyry A (2016) Amino alkylated indoles as corrosion inhibitors for mild steel in 1M HCl: experimental and theoretical studies. J Mol Liq 219:647–660

6. Vinutha MR, Venkatesha TV (2016) Review on mechanistic action of inhibitors on steel corrosion in acidic media. Port Electrochim Acta 34(3):157–184

7. Ghazoui A, Saddik R, Hammouti B, Zarrouk A, Benchat N, Guenbour M, Al-Deyab SS, Warad I (2013) Inhibitive effect of imidazopyridine derivative towards corrosion of C38 steel in hydrochloric acid solution. Res Chem Intermed 39(6):2369–2377

8. Yadav M, Behera D, Kumar S (2014) Experimental and theoretical investigation on adsorption and corrosion inhibition properties of imidazopyridine derivatives on mild steel in hydrochloric acid solution. Surf Interface Anal 46(9):640–652

9. Bourichi S, Kandri Rodi Y, EL Azzouzi M, Kharbach Y, Ouazzani Chahdi F, Aouniti A (2017) Inhibitive effect of new synthetized imidazopyridine derivatives for the mild steel corrosion in Hydrochloric acid medium. J Mater Environ Sci 8(5):1696–1707

10. AL Jahdaly BA, Awad MI (2016) Enhanced inhibition of corrosion of mild steel by triazole derivative in presence of copper ions. Int J Electrochem Sci 11(7):5473–5480

11. Anejjar A, Salghi R, Zarrouk A, Zarrok H, Benali O, Hammouti B, Al-Deyab SS, Benchat N, Saddik R (2015) Investigation of inhibition by 6-bromo-3-nitroso-2-phenylimidazol[1,2-α]pyridine of the corrosion of C38 steel in 1 M HCl. Res Chem Intermed 41(2):913–925

12. Ech-chihbi E, Salim R, Oudda H, Elaatiaoui A, Rais Z, Oussaid A, El Hajjaji F, Hammouti B, Elmsellem H, Taleb M (2016) Effect of some imidazopyridine compounds on carbon steel corrosion in hydrochloric acid solution. Der Pharma Chem 8(13):214–230

13. Tatipaka HB, Gillespie JR, Chatterjee KA, Norcross RN, Hulverson MA, Ranade RM, Nagendar P, Creason SA, McQueen J, Duster NA, Nagle A, Supek F, Molteni V, Wenzler T, Brun R, Glynne R, Buckner FS, Gelb MH (2014) Substituted 2-phenylimidazopyridines: a new class of drug leads for human african trypanosomiasis. J Med Chem 57(3):828–835

14. Anaflous A, Benchat N, Mimouni M, Abouricha S, Ben-Hadda T, El-Bali B, Hakkou A, Hacht B (2004) Armed imidazo [1,2-a] pyrimidines (pyridines): evaluation of antibacterial activity. Lett Drug Des Discov 1(3):224–229

15. Kosari A, Moayed MH, Davoodi A, Parvizi R, Momeni M, Eshghi H, Moradi H (2014) Electrochemical and quantum chemical assessment of two organic compounds from pyridine derivatives as corrosion inhibitors for mild steel in HCl solution under stagnant condition and hydrodynamic flow. Corros Sci 78:138–150

16. Ismaily Alaoui K, El Hajjaji F, Azaroual M, Taleb M, Chetouani A, Hammouti B, Abrigach F, Khoutoul M, Abboud Y, Aouniti A, Touzani R (2014) Experimental and quantum chemical studies on corrosion inhibition performance of pyrazolic derivatives for mild steel in hydrochloric acid medium, correlation between electronic structure and inhibition efficiency. J Chem Pharm Res 6(7):63–81

17. Kumar R, Chahal S, Kumar S, Lata S, Lgaz H, Salghi R, Jodeh SJ (2017) Corrosion inhibition performance of chromone-3-acrylic acid derivatives for low alloy steel with theoretical modeling and experimental aspects. J Mol Liq 243:439–450

18. Elhousni L, Galai M, ElKamraoui FZ, Dkhireche N, EbnTouhami M, Touir R, Chebabe D, Sfaira M, Zarrouk A (2016) Study of sodium gluconate and cetyltrimethyl ammonium bromide as inhibitor for copper in Moroccan industrial cooling water systems. J Mater Environ Sci 7(7):2513–2525

19. Saqalli L, Galai M, Benhiba F, Gharda N, Habbadi Ghailane NR, EbnTouhami M, Peres-lucchese Y, Souizi A, Touir R (2017) Experimental and theoretical studies of Alizarin as corrosion inhibitor for mild steel in 1.0 M HCl solution. J Mater Environ Sci 8(7):2455–2468

20. El-Hajjaji F, Zerga B, Sfaira M, Taleb M, EbnTouhami M, Hammouti B, Al-Deyab S, Benzeid H, El Essassi M (2014) Comparative study of novel N-substituted quinoxaline derivatives towards mild steel corrosion in hydrochloric acid: part 1. J Mater Environ Sci 5(1):255–262

21. Bouoidina A, Chaouch M, Abdellaoui A, Lahkimi A, Hammouti B, El-Hajjaji F, Taleb M, Nahle A (2017) Essential oil of "Foeniculumvulgare": antioxidant and corrosion inhibitor on mild steel immersed in hydrochloric medium. Anti-Corros Methods Mater 64(5):563–572

22. El-Hajjaji F, Belghiti ME, Hammouti B, Jodeh S, Hamed O, Lgaz H, Salghi R (2018) Adsorption and corrosion inhibition effect of 2-mercaptobenzimidazole (surfactant) on a carbon steel surface in an acidic medium: experimental and monte carlo simulations. Port Electrochim Acta 36(3):197–212

23. Nahle A, El-Hajjaji F, Ghazoui A, Benchat N, Taleb M, Saddik R, Elaatiaoui A, Koudad M, Hammouti B (2018) Effect of substituted methyl group by phenyl group in pyridazine ring on the corrosion inhibition of mild steel in 1.0 M HCl. Anti-Corros Methods Mater 65(1):87–96

24. Lgaz H, Subrahmanya Bhat K, Salghi R, Shubhalaxmi, Jodeh S, Algarra M, Hammouti B, Hassan Ali I, Essamri A (2017) Insights into corrosion inhibition behavior of three chalcone derivatives for mild steel in hydrochloric acid solution. J Mol Liq 238:71–83

25. El Hattabi L, Echihi S, El Fal M, Guenbour A, Ramli Y, Essassi EM, Tabyaoui M (2017) Electrochemical and quantum chemical study of 1-ethyl-1H-pyrazolo [3,4-d] pyrimidine-4(5H)-thione as corrosion inhibitor for mild steel in HCl solution. J Mater Environ Sci 8(7):2428–2441

26. Singh A, Ansari KR, Kumar A, Liu W, Songsong C, Lin Y (2017) Electrochemical, surface and quantum chemical studies of novel imidazole derivatives as corrosion inhibitors for J55 steel in sweet corrosive environment. J Alloy Compd 712:121–133

27. Zarrouk A, Hammouti B, Dafali A, Bouachrine M, Zarrok H, Boukhris S, Salem Al-Deyab S (2014) A theoretical study on the inhibition efficiencies of some quinoxalines as corrosion inhibitors of copper in nitric acid. J Saudi Chem Soc 18(5):450–455

28. Hamani H, Douadi T, Daoud D, Al-Noaimi M, Rikkouh RA, Chafaa S (2017) 1-(4-Nitrophenylo-imino)-1-(phenylhydrazono)-propan-2-one as corrosion inhibitor for mild steel in 1 M HCl solution: weight loss, electrochemical, thermodynamic and quantum chemical studies. J Electroanal Chem 801:425–438

29. Zarrouk A, Zarrok H, Salghi R, Hammouti B, Bentiss F, Touir R, Bouachrine M (2013) Evaluation of N-containing organic compound as corrosion inhibitor for carbon steel in phosphoric acid. J Mater Environ Sci 4(2):177–192

30. Bentiss F, Outirite M, Traisnel M, Vezin H, Lagrenée M, Hammouti B, Al-Deyab SS, Jama C (2012) Improvement of corrosion resistance of carbon steel in hydrochloric acid medium by 3,6-bis(3-pyridyl)pyridazine. Int J Electrochem Sci 7(2):1699–1723

31. Hazwan Hussin M, Jain Kassim M (2011) The corrosion inhibition and adsorption behavior of Uncaria gambir extract on mild steel in 1 M HCl. Mater Chem Phys 125(3):461–468

32. Markhali BP, Naderi R, Mahdavian M, Sayebani M, Arman SY (2013) Electrochemical impedance spectroscopy and electrochemical noise measurements as tools to evaluate corrosion inhibition of azole compounds on stainless steel in acidic media. Corros Sci 75:269–279

33. Haque J, Srivastava V, Verma C, Quraishi MA (2017) Experimental and quantum chemical analysis of 2-amino-3-((4-((S)-2-amino-2-carboxyethyl)-1H-imidazol-2-yl)thio)propionic acid as new and green corrosion inhibitor for mild steel in 1 M hydrochloric acid solution. J Mol Liq 225:848–855

34. Rbaa M, Galai M, Kacimi YE, Ouakki M, Touir R, Lakhrissi B, EbnTouhami M (2017) Adsorption properties and inhibition of carbon steel corrosion in a hydrochloric solution by 2-(4,5-diphenyl-4,5-dihydro-1h-imidazol-2-yl)-5-methoxyphenol. Port Electrochim Acta 35(6):323–338

35. Abd El-Raouf M, Khamis E, Abou Kana A, Negm MTH NA (2018) Electrochemical and quantum chemical evaluation of new bis(coumarins) derivatives as corrosion inhibitors for carbon steel corrosion in 0.5 M H_2SO_4. J Mol Liq 255:341–353

36. Hamani H, Douadi T, Al-Noaimi M, Issaadi S, Daoud D, Chafaa S (2014) Electrochemical and quantum chemical studies of some azomethine compounds as corrosion inhibitors for mild steel in 1 M hydrochloric acid. Corros Sci 88:234–245

37. Ribeiro DV, Abrantes JCC (2016) Application of electrochemical impedance spectroscopy (EIS) to monitor the corrosion of reinforced concrete: a new approach. Constr Build Mater 111:98–104

38. Mohamed Abdelahi MM, Elmsellem H, Benchidmi M, Sebbar NK, Belghiti MA, El Ouasif L, Jilalat AE, Kadmi Y, Essassi EM (2017) A DFT and molecular dynamics study on inhibitory action of indazole derivative on corrosion of mild steel. J Mater Environ Sci 8(5):1860–1876

39. Hamani H, Douadi T, Al-Noaimi M, Issaadi S, Daoud D, Chafaa S (2014) Electrochemical and quantum chemical studies of some azomethine compounds as corrosion inhibitors for mild steel in 1M hydrochloric acid. Corros Sci 88:234–245

40. Elmsellem H, Youssouf MH, Aouniti A, Ben Hadda T, Chetouani A, Hammouti B (2014) Adsorption and inhibition effect of curcumin on mild steel corrosion in hydrochloric acid. J Appl Chem 87(6):744–753

41. Solmaz R (2014) Investigation of adsorption and corrosion inhibition of mild steel in hydrochloric acid solution by 5-(4-dimethyl-aminobenzylidene)rhodanine. Corros Sci 79:169–176

42. Galai M, El Faydy M, El Kacimi Y, Dahmani K, Alaoui K, Touir R, Lakhrissi B, EbnTouhami M (2017) Synthesis, characterization and anti-corrosion properties of novel quinolinol on C-steel in a molar hydrochloric acid solution. Port Electrochim Acta 35(4):233–251

43. Ahamad I, Prasad R, Quraishi MA (2010) Adsorption and inhibitive properties of some new Mannich bases of Isatin derivatives on corrosion of mild steel in acidic media. Corros Sci 52(4):1472–1481

44. El-Hajjaji F, Messali FM, Aljuhani A, Aouad MR, Hammouti B, Belghiti ME, Chauhan DS, Quraishi MA (2018) Pyridazinium-based ionic liquids as novel and green corrosion inhibitors of carbon steel in acid medium: electrochemical and molecular dynamics simulation studies. J Mol Liq 249:997–1008

45. Abd-El-Nabey BA, El-Housseiny S, El-Naggar GA, Matter EA, Esmail G (2015) Inhibitive action of alhagi maurorum plant extract on the corrosion of copper in 0.5 M H_2SO_4. Phys Chem 5(3):49–62

46. Fdil R, Tourabi M, Derhali S, Mouzdahir A, Sraidi k, Jama C, Zarrouk A, Bentiss F (2018) Evaluation of alkaloids extract of *Retama monosperma* (L.) Boiss. stems as a green corrosion inhibitor for carbon steel in pickling acidic medium by means of gravimetric, AC impedance and surface studies. J Mater Environ Sci 9(1):358–369

47. Ech-chihbi E, Belghiti ME, Salim R, Oudda H, Taleb M, Benchat N, Hammouti B, El-Hajjaji F (2017) Experimental and computational studies on the inhibition performance of the organic compound "2-phenylimidazo [1,2-a]pyrimidine-3-carbaldehyde" against the corrosion of carbon steel in 1.0 M HCl solution. Surf Interfaces 9:206–217

48. Ameer MA, Fekry AM, Othman A (2014) Electrochemical investigation of green inhibitor adsorption on low-carbon steel in produced water. Int J Electrochem Sci 9(4):1964–1985

49. Deyab MA, Abd El-Rehim SS (2013) Influence of polyethylene glycols on the corrosion inhibition of carbon steel in butyric acid solution: weight loss, EIS and theoretical studies. Int J Electrochem Sci 8(12):12613–12627

50. El-Tabei AS, Elsharaky EA, El-Tabey AE (2016) A comparative the inhibition performance of a newly synthesized cationic surfmer and its oligomer surfactant for carbon steel corrosion in 1M acid chloride solution. Int J Electrochem Sci 11(12):10978–11001

51. Bendjeddou A, Abbaz T, Gouasmia A, Villemin K D (2016) Molecular structure, HOMO-LUMO, MEP and Fukui function analysis of some TTF-donor substituted molecules using DFT (B3LYP) calculations. Int Res J Pure Appl Chem 12(1):1–9

52. Raja G, Saravanan K, Sivakumar S (2015) Quantum chemical investigations on benzene derivative: a DFT study. Rasayan J Chem 8(1):37–41

53. Fouda AS, Mohamed FSH, El-Sherbeni MW (2016) Corrosion inhibition of aluminum–silicon alloy in hydrochloric acid solutions using carbamidic thioanhydride derivatives. J Bio-Tribo-Corros 2:11. https://doi.org/10.1007/s40735-016-0039-y

54. Belghiti ME, Karzazi Y, Tighadouini S, Dafali A, Jama C, Warad I, Hammouti B, Radi S (2016) New hydrazine derivatives as corrosion for mild steel in phosphoric acid medium. Part B: theoretical investigation. J Mater Environ Sci 7(3):956–967

55. Karzazi Y, El Alaoui Belghiti M, Dafali A, Hammouti B (2014) A theoretical investigation on the corrosion inhibition of mild steel by piperidine derivatives in hydrochloric acid solution. J Chem Pharm Res 6(4):689–696

56. Ibeji CU, Adejoro IA, Adeleke BB (2015) A benchmark study on the properties of unsubstituted and some substituted polypyrroles. J Phys Chem Biophys 5(6):193/1–193/11

57. Sayin K, Karakas D (2017) Ab-initio and DFT calculations on some inorganic inhibitors computational study on inorganic corrosion inhibitors. J New Results Sci 6(1):20–31

58. Zarrouk A, Hammouti B, Dafali A, Bouachrine M, Zarrok H, Boukjris S, Al-Deyab SS (2014) A theoretical study on the inhibition efficiencies of some quinoxalines as corrosion inhibitors of copper in nitric acid. J Saudi Chem Soc 8(5):450–455

59. Yadav M, Kumar S, Sinha RR, Behera D (2013) Experimental and quantum chemical studies on the corrosion inhibition performance of benzimidazole derivatives for mild steel in HCl. Ind Eng Chem Res 52(19): 6318–6328

60. Obot IB, Gasem ZM, Umoren SA (2014) Understanding the mechanism of 2-mercaptobenzimidazole adsorption on Fe (110), Cu (111) and Al (111) surfaces: DFT and molecular dynamics simulations approaches. Int J Electrochem Sci 9(5):2367–2378

61. Yadav M, Behera D, Kumar S, Sinha R (2013) Experimental and quantum chemical studies on the corrosion inhibition performance of benzimidazole derivatives for mild steel in HCl. Ind Eng Chem Res 52(19):6318–6328

62. Zhang Z, Tian N, Zhang L, Wu L Inhibition of the corrosion of carbon steel in HCl solution by methionine and its derivatives. Corros. Sci. 98: 438–449

63. Obot IB, Gasem ZM (2014) Theoretical evaluation of corrosion inhibition performance of some pyrazine derivatives. Corros Sci 83:359–366

64. Bedair MA (2016) The effect of structure parameters on the corrosion inhibition effect of some heterocyclic nitrogen organic compounds. J Mol Liq 219:128–141

65. Roque JM, Pandiyan T, Cruz J, Garcı´a-Ochoa E (2008) DFT and electrochemical studies of tris(benzimidazole-2-ylmethyl)amine as an efficient corrosion inhibitor for carbon steel surface. Corros Sci 50(3):614–624

66. El Ibrahimi B, Soumoue A, Jmiai A, Bourzi H, Oukhrib R, El Mouaden K, El Issami S, Bazzi L (2016) Computational study of some triazole derivatives (un- and protonated forms) and their copper complexes in corrosion inhibition process. J Mol Struct 1125:93–102